# Evaluation of Thermal Deformation Model for BGA Packages Using Moiré Interferometry

**Jinwon Joo***
*School of Mechanical Engineering, Chungbuk National University, Cheongju, Chungbuk, 361-763, Korea*
**Seungmin Cho**
*Department of Mechanical Engineering, University of Maryland College Park, MD 20742, USA*

A compact model approach of a network of spring elements for elastic loading is presented for the thermal deformation analysis of BGA package assembly. High-sensitivity moiré interferometry is applied to evaluate and calibrated the model quantitatively. Two ball grid array (BGA) package assemblies are employed for moiré experiments. For a package assembly with a small global bending, the spring model can predict the boundary conditions of the critical solder ball excellently well. For a package assembly with a large global bending, however, the relative displacements determined by spring model agree well with that by experiment after accounting for the rigid-body rotation. The shear strain results of the FEM with the input from the calibrated compact spring model agree reasonably well with the experimental data. The results imply that the combined approach of the compact spring model and the local FE analysis is an effective way to predict strains and stresses and to determine solder damage of the critical solder ball.

**Key Words :** Moiré Interferometry, BGA Package, Solder Ball, Compact Spring Model, Thermomechanical Behavior, On Board Reliability

## 1. Introduction

An increased use of chip carriers with many small solder interconnections, such as the ball grid array (BGA) package, has been widely reported in recent years. Investigation on failures in solder interconnections becomes more important for reliability assessment of microelectronics. An electronic package assembly comprises various materials that have different thermo-mechanical properties. The nonuniform properties of the silicon die, ceramic carrier, the printed circuit board (PCB) and the solder interconnections produce variations in strain within the BGA package assembly, which is subjected to cyclic loading. An understanding of the thermal response of the various components is critical for improving package design and yielding maximum performance and reliability.

The accelerated thermal cycling test (ACT), in which electronic assemblies are cycled through extremes of temperature, has been used extensively (Darveaux and Mawer, 1995) for assessing thermal fatigue. The measured fatigue life is useful for comparing designs, but provides only limited information about the thermo-mechanical response. The nonlinear behavior, such as the plastic deformation and creep of solder, makes it more difficult to determine the conditions of the ACT, and thus to predict the reliability of

* Corresponding Author,
**E-mail** : jinwon@chungbuk.ac.kr
**TEL** : +82-43-261-2456; **FAX** : +82-43-263-2441
School of Mechanical Engineering, Chungbuk National University, Cheongju, Chungbuk, 361-763, Korea.
(Manuscript **Received** May 10, 2003; **Revised** October 22, 2003)

electronic devices. Finite element analysis can be used (Corbin, 1993 ; Jung et al., 1996 ; Lee et al., 1998) to estimate deformations and stresses in electronic package assemblies. While the finite element method is a useful numerical tool for detailed prediction of deformation of electronical packages, the models and results usually require precise experimental verification.

Moiré interferometry is a full-field optical method that provides high-sensitivity displacement measurement and high spatial resolution (Post et al., 1994). The method has been effectively applied to the research areas of composite material (Guo et al., 1992; Joo et al., 2002a). Recently, the applicability of the method has been extended to thermal deformation analysis of microelectronics devices (Guo et al., 1993 ; Han and Guo, 1995 ; Han, 1998 ; Zhao, 1998 ; Joo and Han, 2002b). In this paper, a compact model approach of a network of spring elements for elastic loading is presented for the thermal deformation analysis of BGA package assembly. High-sensitivity moiré interferometry is applied to evaluate and calibrate the model quantitatively. Two ball grid array (BGA) package assembly are employed for moiré experiments : a small ceramic BGA package (81 I/Os) assembly and a large ceramic BGA package (361 I/Os) assembly. Shear strains of the solder ball as well as horizontal displacements of the package and the PCB due to temperature change are documented.

## 2. Thermal Deformation of BGA Packages

Ball grid array (BGA) package assembly consists mainly of module, printed circuit board (PCB) and solder interconnections that connect the module and PCB. Solder inlerconnections are arranged in a square array. The thermal deformations are induced by a mismatch of coefficients of thermal expansion (CTE) between the module and the PCB. The effect of CTE mismatch is illustrated in Fig. 1. When the package assembly is heated from a room temperature, the PCB expands more than the ceramic module by

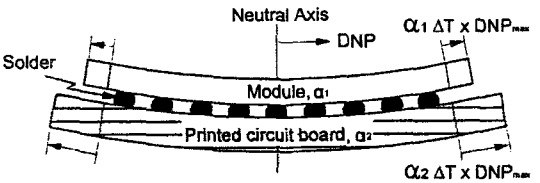


**Fig. 1** Global deformation of BGA package assembly due to temperature change

$$U_2-U_1=(\alpha_2-\alpha_1)\times\Delta T\times DNP_{\max} \quad (1)$$

where $\alpha_2$ and $\alpha_1$ are the CTE values of the module and the PCB, respectively, $\Delta T$ is the temperature change and $DNP_{\max}$ is the maximum distance from the neutral point. This uneven expansion produces not only a bending of the whole assembly but also relative horizontal displacements, resulting in a shear strain of the solder interconnection. The shear stress or the shear strain of solder interconnection is known to be one of the major causes for the failure of microelectronics package assemblies.

A simple equation $\gamma=(U_2-U_1)/h$ ($h$ is the height of solder) for the average shear strain is practically used to assess the reliability of solder interconnections. This equation is, however, not applicable to the area array packages such as BGA package, due to the shear stiffness of solders. The relative displacement between the module and the PCB increases as DNP increases, so that the largest shear strain occurs at the rightmost solder ball. For thermal cycling, the rightmost or the leftmost solder balls are the critical joints expected to fail first. For computational efficiency, only the critical solder ball of a package assembly might be modeled using approximate theoretical analysis or conventional finite element analysis. For the complicated and repeated analysis of critical solder ball considering thermal fatigue and viscoelastic behavior, the load sharing offered by the remaining non-critical solder balls can be modeled with a compact spring model.

The spring compact model consists of a network of spring elements for elastic loading as shown in Fig. 2. It is assumed in the compact spring model that the non-critical solder inter-

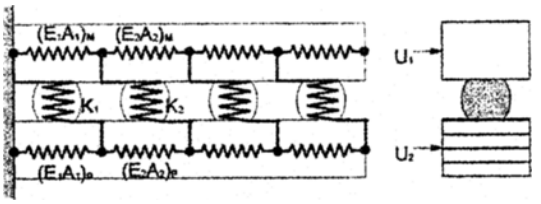


**Fig. 2** Network of compact spring model for the determination of thermal displacement of package assembly

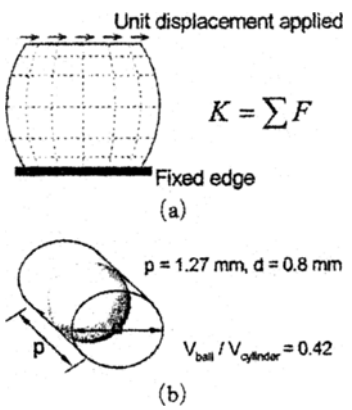


**Fig. 3** Shear stiffness of solder ball calculated by the finite element analysis

connections carry only shear loading and the package and PCB do not experience bending deformation. The package, PCB and solder interconnections are assumed to have elastic behavior, represented by effective properties. The only degrees of freedom in the compact model that need to be retained are those where the model is connected to the detailed model of the critical solder interconnection. All the remaining degree of freedoms internal to the compact model can be eliminated using static condensation techniques. The output of the compact model, $U_1$ and $U_2$ in Fig. 2 can be imposed on the thermal analysis model of the critical solder ball as prescribed displacements. In the compact model approach, the shear stiffness of each solder balls, $K_i$ is calculated by the finite element analysis as shown in Fig. 3(a). The lower surface of the solder being constrained against movement, unit horizontal displacement is applied at nodes along the upper surface. The shear stiffness of the solder was

**Table 1** Elastic modulus and coefficient of thermal expansion of CBGA package assembly

| Part | Elastic modulus (GPa) | CTE (ppm/℃) |
|---|---|---|
| Ceramic | 296.0 | 5.8 |
| PCB | 19.7 | 19.5 |
| High melting solder | 9.9 | 24.0 |
| Eutectic solder | 35.8 | 21.0 |

determined by a summation of the forces of the nodes. Since the maximum cross section of the solder, however, was modeled in the two-dimensional finite element analysis, the difference in volume between a cylinder modeled in the finite element analysis and a real solder ball is compensated in calculating the stiffness as shown in Fig. 3(b).

In this paper, ceramic BGA package assemblies are employed for the thermal deformation analysis. The material properties of the Young's modulus and CTEs used for the analysis of the compact model are listed in Table 1.

## 3. Experimental Approach

### 3.1 Moiré interferometry

Moiré interferometry is an optical method, providing whole field contour maps of in-plane displacements with a sub-wavelength sensitivity. In moiré interferometry, a high-frequency (1200 lines/mm) diffraction grating is replicated on the surface of the specimen and it deforms together with the underlying specimen. The resulting fringe patterns represent contours of constant $U$ and $V$ displacement fields, defined as in-plane displacements in orthogonal $x$ and $y$ directions, respectively. The displacements are determined from the fringe orders by

$$U(x, y) = \frac{1}{2f_s} N_x(x, y)$$
$$V(x, y) = \frac{1}{2f_s} N_y(x, y) \quad (2)$$

where $N_x$ and $N_y$ are fringe orders in the $U$ and $V$ field patterns, respectively. In routine practice, a specimen grating with a frequency $f_s$

of 1200 lines/mm is used, which provides a displacement sensitivity of 0.417 $\mu$m per fringe order.

Shear strain and rotational angle can be calculated by small-strain relationships from the measured displacement fields,

$$\gamma_{xy}=\left[\frac{\partial U}{\partial y}+\frac{\partial V}{\partial x}\right]=\frac{1}{2f_s}\left[\frac{\partial N_y}{\partial x}+\frac{\partial N_x}{\partial y}\right]$$
$$\phi_{xy}=\frac{1}{2}\left[\frac{\partial U}{\partial y}-\frac{\partial V}{\partial x}\right]=\frac{1}{4f_s}\left[\frac{\partial N_y}{\partial x}-\frac{\partial N_x}{\partial y}\right] \quad (3)$$

Real-time moiré interferometry (Cho et al., 2002) was applied for the measurement of in-plane displacements produced by the temperature changes. This technique is capable of documenting thermally induced deformations as a function of temperature and time with sub-micro meter displacement sensitivity. A compact moiré interferometry system (PEMI II, Photomechanics, Inc) was utilized in this experiment. For preventing inadvertent vibrations, the specimen is mechanically isolated from the environmental chamber by a specimen holder being connected only to the moiré system.

### 3.2 Specimens

Two ceramic ball grid array (CBGA) package assemblies were employed for moiré experiments: a small CBGA package assembly which has 81 I/Os and a large CBGA package assembly which has 361 I/Os.

A small CBGA package assembly (CBGA9) containing 9×9 solders was trimmed from a full package assembly (19×19 solders) for a negligible small global bending induced by the temperature change, which would lead to accord with the assumption that the flexures of the component and PCB are not considered in the compact spring model. The ceramic module and the PCB are 12×12 mm square and are 1.50 mm and 2.06 mm thick, respectively. The solder interconnections of the package assembly consists of a high melting point solder ball (90%Pb-10% Sn) and an eutectic fillet (63%Sn-37%Pb), with which solder ball is connected to a ceramic module and a PCB. The solder ball is 0.89 mm high and its diameter is 0.64 mm.

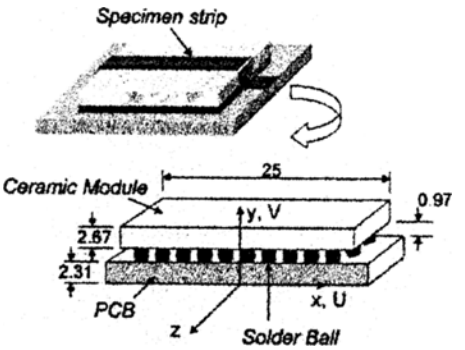


**Fig. 4** Schematic diagram of the ceramic BGA package assembly geometry with relevant dimensions (mm)

A large CBGA package assembly (CBGA19) was sectioned from a full package assembly having 19×19 solder balls to a strip containing central five rows of solder balls. The module and PCB are 25 mm long and are 2.67 mm and 2.31 mm thick, respectively. The solder ball is 0.97 mm high and its diameter is 0.89 mm. A cross section of the CBGA package assembly is shown in Fig. 4 with relevant dimensions. One side of the specimens was ground flat to expose the largest cross section of the solder ball for specimen grating replication. A high frequency (1200 lines/mm) crossed-line diffraction grating was replicated on the surface of the specimen at room temperature.

### 3.3 Experimental procedure and fringe patterns

Real time moiré interferometry was conducted for the measurement of in-plane displacements produced by the temperature changes. Figure 5 depicts the temperature profile used in the experiment for the CGBA package assembly. The specimen was heated in the environmental chamber from room temperature of 24℃ and subjected to approximately one thermal cycles. The maximum and minimum temperature was 122℃ and -20℃, respectively for the small CBGA package assembly, and 100℃ and −20℃ for the large one. The heating rate and cooling rate were 7.25℃/min and 14.5℃/min, respectively, and a dwell time of 10 min was used at the peak temperature.

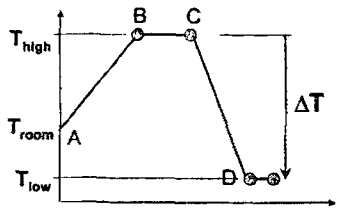


**Fig. 5** Temperature profile used in the experiment of the ceramic BGA package assembly

During the temperature excursion, the fringe patterns were recorded at four selected points of time indicated by A, B, C and D in Fig. 5. The corresponding $U$ and $V$ displacement field patterns for the small CBGA package assembly are shown in Fig. 6. The eutectic solder fillet has a much lower melting point than the high melting solder ball, and thus a large inelastic deformation of solder including time independent plasticity and creep, would occur at an elevated temperature during heating. The inelastic deformation would continue to increase during the dwell time. If the eutectic solders were totally relaxed, the module and the PCB would deform freely without bending. The $U$ and $V$ field patterns at time B show eutectic solders were nearly relaxed and each of the module and the PCB extended almost freely by the temperature change. This thermo-mechanical behavior of the package assembly makes it possible to determine the CTE of each material. The CTE of the ceramic module and the effective CTE of the PCB were determined from the $U$ field moiré fringe pattern at time B by

$$CTE=\frac{1}{f}\frac{\Delta N}{\Delta L \Delta T} \tag{4}$$

where $f$ is a virtual reference frequency (=2400 lines/mm) of the moiré interferometry, $\Delta N$ is the change of fringe orders in the moiré pattern, $\Delta L$ is any gage length across which $\Delta N$ is determined and $\Delta T$ is the temperature change on Celsius scale.

When the package assembly is cooled down quickly, the opposite bending occurs in the package assembly due to the temperature change as shown in the fringe pattern at the time D and it is expected that the eutectic solder ball do not undergo inelastic deformation anymore. Since the

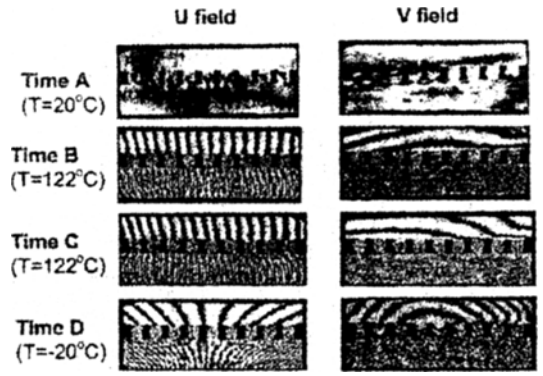


**Fig. 6** U and V displacement field patterns of the small ceramic BGA package assembly (CBGA 9)

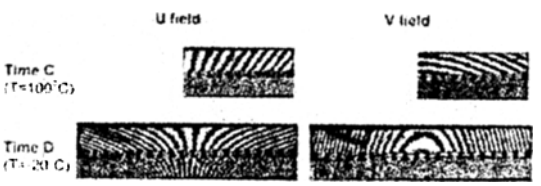


**Fig. 7** U and V displacement field patterns of the large ceramic BGA package assembly (CBGA 19)

package, PCB and solder ball are assumed to have elastic behavior in the compact model approach, the displacements between the time C and D were compared with the displacements calculated by compact model.

Figure 7 shows the corresponding $U$ and $V$ displacement field patterns of the large CBGA package assmbly at temperature C and D in Fig. 5. As the case of the small CBGA package assembly, the opposite bending occurs in the package assembly due to the temperature change. The patterns show large global bending of the module and the PCB. The $U$ displacements between the time C and D were compared with the displacements calculated by the compact spring model.

### 3.4 Fringe analysis of the solder ball

In order to compare strain contours from the finite element analysis with the moiré data, two-dimensional least square fitting was performed for obtaining the displacement field of fringe

patterns. In this process, the displacement $U$ and $V$ is assumed to be summation of monomial functions up to sixth order of $x$ and $y$ as following equations.

$$U(x, y)=\sum_{i=1}^{M}A_iP_i(x, y)$$
$$V(x, y)=\sum_{i=1}^{M}B_iQ_i(x, y) \quad (5)$$

where $M$ is the number monomial functions. Square error is defined as

$$E=\sum_{i=1}^{N}[U(x_i, y_i)-U_i]^2 \quad (6)$$

where $N$ represents the number of points which are picked at the center of each dark fringe. After minimization of square errors, coefficients $A_i$ and $B_i$ can be determined by the linear algebraic equations

$$\sum_{k=1}^{M}\left[\left(\sum_{i=1}^{N}P_k(x_i, y_i)P_m(x_i, y_i)\right)A_k\right]=\sum_{i=1}^{N}P_m(x_i, y_i)U_i,\ m=1, \cdots, M \quad (7)$$

Figure 8 shows displacement fringe patterns of the rightmost solder of the CBGA9 at time C, together with the fitted displacement contours. In both the fringe patterns and the fitted contours, the interval between two adjacent fringes represents displacement of 0.417 $\mu$m. It is seen that the fitted displacement contours are in excellent agreement with the moiré fringe patterns. The strain function can be extracted from the displacement functions by the relationships for small strains.

$$\gamma_{xy}(x, y)=\frac{\partial U}{\partial y}+\frac{\partial V}{\partial x}=\sum_{i=1}^{M}\left[A_i\frac{\partial P_i(x, y)}{\partial y}\right]+\sum_{i=1}^{M}\left[B_i\frac{\partial Q_i(x, y)}{\partial x}\right] \quad (8)$$

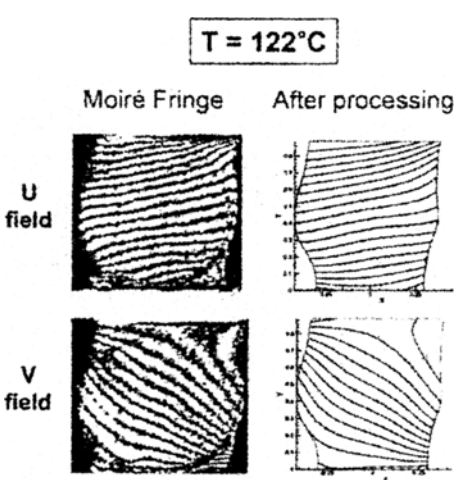


**Fig. 8** Moiré fringe patterns and fitted displacement contours of the rightmost solder ball of ceramic BGA package assembly

## 4. Results and Discussions

Both the horizontal displacements, $U$, from the experiment and the compact spring model increase linearly according to the distance from the neutral point (DNP), and then the maximum horizontal displacement occurs at surfaces connecting the rightmost solder joint. The deformation in the ceramic module is much smaller than that in the PCB, because the material of ceramic has lower CTE and higher Young's modulus than that of PCB. The relative displacements between the module and the PCB cause the shear strain and the shear stress in corresponding solder joints.

The $U$ and $V$ displacement field patterns of the small CBGA package assembly at time C in Fig. 6 show little bending of the module and the PCB. This reveals that the eutectic solders were nearly relaxed and each of the module and the PCB extended almost freely by the temperature change. The CTE of the ceramic module and the effective CTE of the PCB determined by Eq. (4) were 5.8 ppm/℃ and 19.5 ppm/℃, respectively.

During cooling, the CTE mismatch produced the convex upward bending of the assembly, since the reference temperature of zero bending displacement was changed to 122℃. The horizontal $U$ displacements along the center line of the ceramic module and the PCB are shown in Fig. 9, where the CTE values obtained from the moiré data were used in the compact spring model. It should be noted that the theoretical prediction matched with the experimental data very well. The maximum horizontal displacement at the rightmost node calculated from the compact

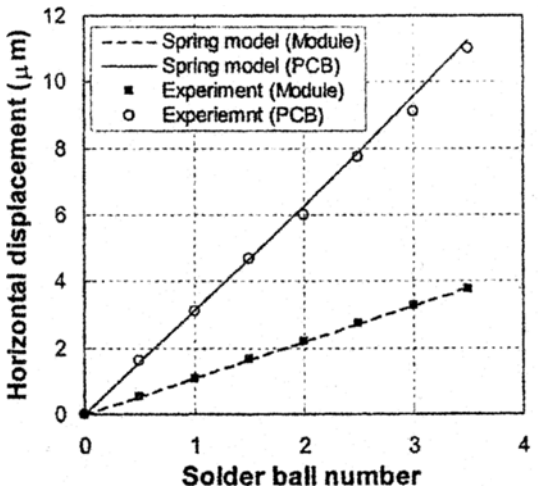


**Fig. 9** Comparison of horizontal displacement of the small ceramic BGA package assembly (CBGA9)

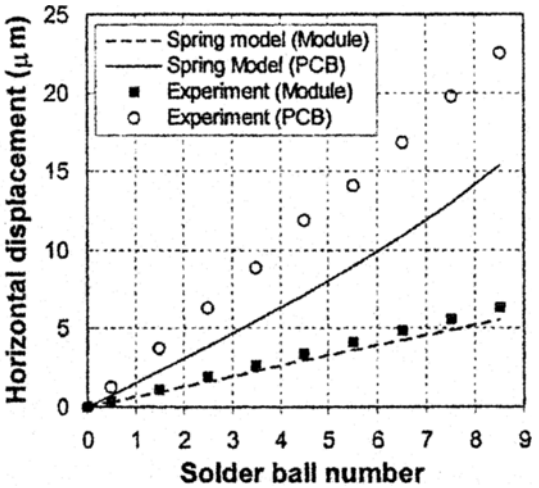


**Fig. 10** Comparison of horizontal displacement of the large ceramic BGA package assembly (CBGA19)

model was 3.80 $\mu$m for the module and 11.24 $\mu$m for the PCB, whereas that from experimental results was 3.79 $\mu$m for the module and 11.03 $\mu$m for the PCB. Consequently, for a package assembly with a small global bending, the compact model can predict the boundary conditions of the critical solder ball extremely well.

The fringe patterns of the large CBGA package assembly at time C in Fig. 7 are saying expansion of the whole assembly due to the temperature increase and those at time D are saying contraction due to temperature decrease with respect to room temperature. The horizontal $U$ displacements of the CBGA19 from the compact spring model from the temperature C to the temperature D were compared with those obtained from the moiré data. Figure 10 shows the horizontal displacements along the centerline of the ceramic module and the PCB. It reveals that the horizontal displacements of the module and the PCB obtained from the spring model are much smaller than those from the moiré data. This discrepancy would be caused mainly by bending effect of the module and the PCB.

The $U$ and $V$ field patterns at time C and D in Fig. 7 show large global bending in the module and the PCB. In order to determine only the stress-induced part of displacement for strain

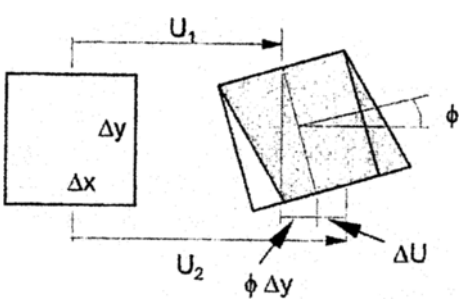


**Fig. 11** Relative horizontal displacement considering rigid body rotation

analysis of the critical solder interconnection, the bending effect was removed from the relative horizontal displacement between the substrate and the PCB as shown in Fig. 11. When a rectangular that has small area of $\Delta x$ by $\Delta y$ rotates by a angle of $\Phi$, the relative displacement due to the rigid body rotation between the top and the bottom lines is $\Phi\Delta y$. Accordingly, the relative displacement that cause the shear strain in solders can be determined from the $U$ and $V$ moiré fringe patterns by

$$\Delta U = U_2 - U_1 - \phi\Delta y$$
$$\text{and } \phi = \frac{1}{2}\left(\frac{\Delta V}{\Delta x} - \frac{\Delta U}{\Delta y}\right) \tag{9}$$

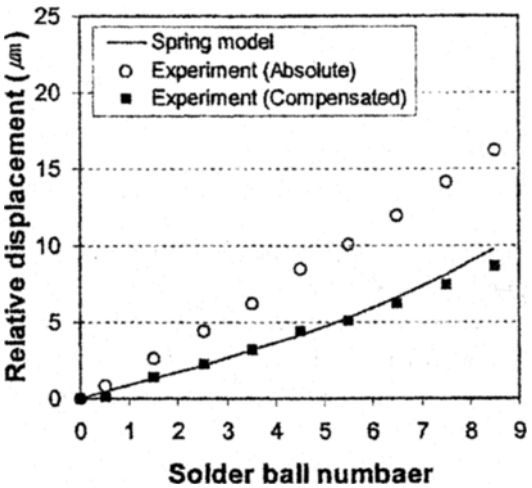


**Fig. 12** Comparison of relative horizontal displacement of the large ceramic BGA package assembly (CBGA19)

where $U_1$ and $U_2$ represent the horizontal displacement at the top and bottom line of the solder, respectively.

Figure 12 shows the relative horizontal displacement between the centerlines of the ceramic module and the PCB determined by Eq. (9). As can be seen from the figure, the relative displacement increased as the DNP increased. It is seen that the experimental relative displacement compensated for the bending effect is in excellent agreement with the theoretical one from the compact spring model. Consequently, for a package assembly with a large global bending, a new compact element is required to account for the rigid-body displacements induced by the global bending.

To characterize the shear strain distribution in the critical solder ball, the corresponding finite element analysis was conducted using the displacement boundary conditions obtained from the experimentally verified compact spring model. The present problem was solved as a plane stress condition considering temperature dependent elastic-plastic deformation. The results were compared with the strains obtained from the moiré experiments. Figure 13 shows contour plots for shear strain $\gamma_{xy}$ in the critical solder ball of the small ceramic BGA package assembly (CBGA9)

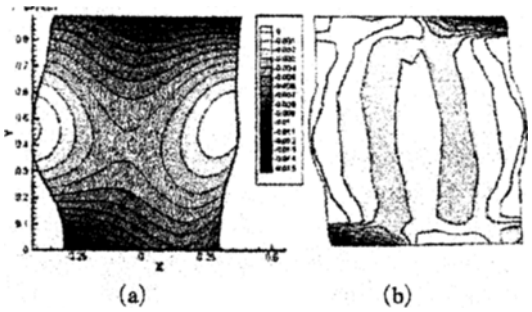


**Fig. 13** Comparison of shear strain distribution on the rightmost solder ball of the CBGA9 obtained by experiment (a) and finite element analysis (b) (Temperature : 122C)

at the elevated temperature of 122℃ (at time C in Fig. 5), which were results of FEM with the input from the compact spring model and results of Eq. (8) with the fitted displacement functions obtained from the moiré experiment.

The shear strain results of FEM agree reasonably well with the experimental data. Fitting process of the experimental data makes the contour more smooth. The high strain areas are in the corner region for both models, with the value for the FEM slightly smaller than that for the experiment. As can be seen in the contour plot, there are considerable differences in the shear strain values between upper right and upper left corners, and maximum strain is located at the upper right or lower left corner in both cases. Upper left and lower right corners of the solder ball always have smaller shear strains. The results from both model satisfy the zero shear strain condition on free surfaces. This non-uniform thermal shear strain distribution in solder balls might be mainly caused by the observation (Guo et al., 1993) that the total shear strain is a sum of the shear strains from the global and local CTE mismatch. The shear strains in the rightmost solder balls from the global and local effect have same sign and are additive at upper right and lower left corners. Consequently, severe shear strain concentration occurred at these regions.

The results imply that the combined approach of the compact spring model and the local FEM is an effective way to predict strains and stresses in the critical solder ball and to determine solder

damage.

## 5. Conclusions

A compact model approach of a network of spring elements for elastic loading is presented for the thermal deformation analysis of BGA package assembly. High-sensitivity moiré interferometry is applied to evaluate the model and calibrated quantitatively. Two ball grid array (BGA) package assemblies are employed for moiré experiments: a small ceramic BGA package (9×9 I/Os) assembly and a big ceramic BGA package (19×19 I/Os) assembly. The experimental data was compared with the numerical predictions to assess the effect of assumptions in the modeling strategies. For a package assembly with a small global bending, the spring model can predict the boundary conditions of the critical solder ball excellently well. For a package assembly with a large global bending, however, the relative displacements determined by spring model agree well with that by experiment after accounting for the rigid-body rotation. The shear strain results of the FEM with the input from the calibrated compact spring model agree reasonably well with the experimental data. The results imply that the combined approach of the compact spring model and the local FEM is an effective way to predict strains and stresses in the critical solder ball and to determine solder damage.

## Acknowledgment

This paper was supported by grant No. R05-2000-000-00304-0 from the Basic Research Program of the Korea Science & Engineering Foundation (KOSEF). The experiment for this paper were performed at the CALCE Electronic Product and System Center of the University of Maryland. Their supports are gratefully acknowledged.

## References

Cho, S. M., Cho, S. Y. and Han, B., 2002, "Observing Real-time Thermal Deformations in Electronic Packaging," *Experimental Techniques*, Vol. 26, No. 3, pp. 25~29.

Corbin, J. S, 1993, "Finite Element Analysis for Solder Ball Connect (SBC) Structural design Optimization," *IBM J. Research Development*, Vol. 37, No. 5, pp. 585~596.

Darveaux, R. and Mawer, A, 1995, "Thermal and Power Cycle Limit of Plastic ball grid array (PBGA) assemblies," *Proc. Surface Mount Int. Conf.*, San Jose, CA, pp. 315~326.

Guo, Y., Post, D. and Han, B., 1992, "Thick Composites in Compression: An Experimental Study of Micro-mechanical Behavior and Smeared Engineering Properties," *J. Composite Material*, Vol. 26, No. 13, pp. 1930~1944.

Guo, Y., Lim, C. K., Chen, W. T. and Woychik, C. G., 1993, "Solder Ball Connect (SBC) Assemblies Under Thermal Loading: I. Deformation Measurement via Moiré Interferometry, and Its Interpretation," *IBM J. Research Development*, Vol. 37, No. 5, pp. 635~648.

Han, B. and Guo, Y., 1995, "Thermal Deformation Analysis of Various Electronic Packaging Products by Moiré and Microscopic Moiré Interferometry," *J. Electronic Packaging, Trans. ASME*, Vol. 117, pp. 185~191.

Han, B., 1998, "Recent Advancements of Moiré and Microscopic Moiré Interferometry for Thermal Deformation Analysis of Microelectrics Devices," *Experimental Mechanics*, Vol. 38, No. 4, pp. 278~288.

Joo, J. W., Chai, S. E. and Shin, D. I., 2002a, "Deformation Analysis of Composite-Patched Concrete Using Moiré Interferometry," *Transactions of the KSME, A*, Vol. 26, No. 1, pp. 160~170.

Joo, J. and Han, B., 2002b, "Thermo-mechanical and Flexural Analysis of WB-PBGA Package Using Moiré Interferometry," *Transactions of the KSME, A*, Vol. 26, No. 7, pp. 1302~1308.

Jung, W., Lau, J. H. and Pao, Y. H., 1996, "Nonlinear Analysis of Full-matrix and Perimeter Plastic Ball Grid Array Solder Joints," *Proc. 1996 ASME International Mechanical Engineering congress & Exhibition*, Atlanta, GA, pp. 1~19.

Lee, T., Lee, J. and Jung, I., 1998, "Finite

Element Analysis for Solder Ball Failures in Chip Scale Packages," *Microelectronics and Reliability*, Vol. 38, No. 12, pp. 1941~1947.

Post, D., Han, B. and Ifju, P., 1994, *High Sensitivity Moiré : Experiental Analysis for Mechanics and Materials*, Springer-Verlag, New York.

Zhao, J.-H., Dai, X. and Ho, P. S., 1998, "Analysis and Modeling Verification for Thermal-mechanical Deformation in Flip-Chip Packages," *Proc. 48th Electronic Components and Technology Conference*, Seattle, WA, May, 1998, pp. 336~344.